

Article

Visualization of Fluoride Ions In Vivo Using a Gadolinium(III)-Coumarin Complex-Based Fluorescence/MRI Dual-Modal Probe

Yue Wang¹, Renfeng Song², Huan Feng¹, Ke Guo², Qingtao Meng^{1,*}, Haijun Chi¹, Run Zhang^{1,3,*} and Zhiqiang Zhang¹

¹ School of Chemical Engineering, University of Science and Technology Liaoning, Anshan 114051, China; Wangyue9088@163.com (Y.W.); FengHuan960421@163.com (H.F.); chi_haijun@163.com (H.C.); henrry1964@163.com (Z.Z.)

² Ansteel Mining Engineering Corporation, Anshan 114002, China; srfandwl@163.com (R.S.); asgk2006@sina.com (K.G.)

³ Australian Institute for Bioengineering and Nanotechnology, The University of Queensland, Brisbane 4072, Australia

* Correspondence: qtmeng@ustl.edu.cn (Q.M.); r.zhang@uq.edu.au (R.Z.); Tel.: +86-412-592-9627 (Q.M.)

Academic Editors: Jong Seung Kim and Min Hee Lee

Received: 17 November 2016; Accepted: 12 December 2016; Published: 16 December 2016

Abstract: A new Gadolinium(III)-coumarin complex, DO3A-Gd-CA, was designed and prepared as a dual-modal probe for simultaneous fluorescence and relaxivity responses to fluoride ions (F^-) in aqueous media and mice. DO3A-Gd-CA was designed by using Gd(III) center as an MRI signal output unit and fluoride binding site, and the 4-(diethylamino)-coumarin-3-carboxylic acid (CA) as a fluorescence reporter. Upon the addition of fluoride ions to the solution of DO3A-Gd-CA, the liberation of the coordinated CA ligand led to a 5.7-fold fluorescence enhancement and a 75% increase in the longitudinal relaxivity (r_1). The fluorescent detection limit for fluoride ions was determined to be $8 \mu M$ based on a $3\sigma/slope$. The desirable features of the proposed DO3A-Gd-CA, such as high sensitivity and specificity, reliability at physiological pH and low cytotoxicity enable its application in visualization of fluoride ion in mice. The successful in vivo imaging indicates that DO3A-Gd-CA could be potentially used in biomedical diagnosis fields.

Keywords: gadolinium(III) complex; dual-modal; detection; fluorescence/MRI; fluoride ion

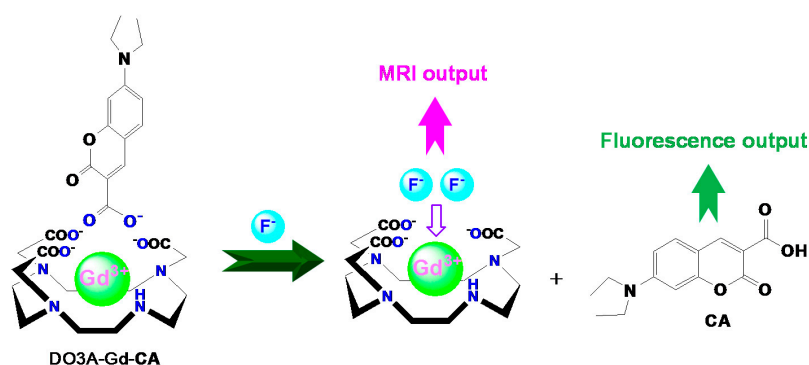
1. Introduction

Detection and diagnosis of diseases at early stage with a high level of accuracy is the key factor to be considered in biomedical and clinical researches on the treatment of diseases [1,2]. The disease biomarkers are often detected at all stages during diseases diagnostic and treatment, while such detection remains a challenge currently [3,4]. Molecular imaging enables visualization of disease biomarkers and their metabolisms in living systems in real time at various levels from molecules and single cells, to tissues, and organs, which allows detection and differential diagnosis of diseases [5,6]. Over the past decades, a variety of molecular imaging techniques, such as positron emission tomography (PET), X-ray computed tomography (CT), magnetic resonance imaging (MRI) and fluorescence imaging (FI), have been widely used in clinical diagnostics, biomedical research and molecular imaging fields [7–10]. Each method has its inherent advantages and considerations. For instance, a magnetic resonance imaging (MRI) technique is characterized by superb spatial resolution but low sensitivity and requires a high concentration of the contrast agent [11]. Fluorescence imaging, on the other hand, has much higher sensitivity and the potential for real-time imaging, but with limited penetration depth of optical photonics, which restricts their application in the

detection of biomarkers in deep tissues [12]. These limitations could be addressed by the dual-modal or multi-modal imaging techniques proposed recently [13–15]. A fluorescence/MRI dual-modal probe fabricated by integrating a fluorescent unit with a contrast agent could thus be used for imaging of biomarkers in vivo. With these dual-modal probes, detailed information on biomarkers in cells and organs within live bodies could be observed simultaneously employing fluorescence imaging and MRI techniques [16]. Therefore, molecular probes, defined as a class of molecules that bind selectively to the analyte of interest with concomitant change in one or more properties of the system, such as fluorescence color [17–19], redox potential and magnetic resonance [20], plays fundamental roles in advanced imaging techniques [21]. In recent years, numerous efforts have been made for the development of molecular probes for the monitoring of biomarkers in biological systems [22]. Nevertheless, to the best of our knowledge, anions fluorescence/MRI dual-modal probes based on Gd(III) complex have been scarcely reported [23].

Due to the important roles of anions played in live organisms, environmental samples, and in the broad applications (e.g., catalysis, etc.), the development of molecular probes for the selective and sensitive sensing and quantification of anions of interest have attracted considerable interest [24]. Among various important anions in biological systems, fluoride ion, being the smallest and most electronegative anion, has particularly attracted attention due to its profound effects on human health. It is well known that intake of acute amount of fluoride ions is beneficial to the treatment of osteoporosis and dental health [25]. On the other hand, excessive intake of fluoride ions may induce various diseases, such as gastrointestinal dysfunction, dental fluorosis, bone fluorosis, and so on [26,27]. Accordingly, the development of molecule probes for the selective and sensitive detection of fluoride ion in biological systems is urgently needed.

In recent years, lanthanide (Ln) complexes have been reported to be an excellent candidate for the development of the responsive optical probes owing to their unique photophysical properties [28–30]. By virtue of the extremely high Ln–fluoride affinity, the coordinated molecules or fluorophores of Ln complexes can be displaced by fluoride ions. As the result of this interaction, the liberation of the coordinated ligands may lead to the changes in several observable signals, such as colour [31], fluorescence and MR [32,33]. Due to their high magnetic moment and symmetric electronic ground state, gadolinium(III) complexes have been frequently chosen as MRI contrast agents [34]. As a consequence of the fluoride ions-induced displacement, the relaxivity of Gd(III) complexes thus could be finely tuned by changing in q (number of coordinated water molecular) upon the addition of targeted fluoride ions in aqueous solution (Scheme 1) [35–43].



Scheme 1. Proposed dual-modal responses mechanism of DO3A-Gd-CA towards fluoride ion.

2. Materials and Methods

2.1. Materials and Instruments

4-Diethylaminosalicylaldehyde, diethylmalonate, piperidine and tetrabutylammonium salts of F^- , Cl^- , Br^- , I^- , HSO_4^- , NO_3^- , OH^- , AcO^- , PO_4^{3-} and $H_2PO_4^-$ were purchased from Sinopharm

Chemical Reagent Co., Ltd. (Shanghai, China). GdCl₃, 1,4,7,10-Tetraazacyclododecane (Cyclen), tert-Butyl bromoacetate and trifluoroacetic acid were purchased from Alfa Aesar.

¹H-NMR and ¹³C-NMR spectra were recorded with an AVANCE600MHZ spectrometer (BRUKER) with chemical shifts reported as ppm (in DMSO, TMS as internal standard). API-ES mass spectra were recorded on an Agilent 6530QTOF spectrometer. Fluorescence spectra were determined with LS 55 luminescence spectrometer (Perkin Elmer, Waltham, MA, USA). The absorption spectra were measured with a Lambda 900 UV/VIS/NIR spectrophotometer (Perkin Elmer, Waltham, MA, USA). Longitudinal relaxivity (*r*₁) and MR imaging were performed on an MesoMR23-060H-I Analyst Analyzing & Imaging system (Shanghai Niumag Corp., Shanghai, China) using a 0.5 T magnet, point resolution = 256 × 128 mm, section thickness = 1 mm, TE = 18.2 ms, TR = 400 ms, and number of acquisitions = 4.

2.2. Synthesis and Characterization of 4-(Diethylamino)-coumarin-3-carboxylic acid (CA)

4-(diethylamino)-coumarin-3-carboxylic acid (CA) was synthesized according to the literature procedure in 78% yield [44]. ¹H-NMR (DMSO-*d*, 600 MHz) δ (ppm): 12.52 (s, H), 8.59 (s, 1H), 7.64 (d, *J* = 12.0 Hz, 2H), 6.79 (d, *J* = 12.0 Hz, 2H), 6.57 (s, 1H), 3.49 (m, *J* = 9.0 Hz, 4H), 1.14 (t, *J* = 9.0 Hz, 6H). ¹³C-NMR (DMSO-*d*, 150 MHz) δ (ppm): 165.0, 160.0, 158.4, 153.4, 149.9, 132.3, 110.5, 107.8, 107.7, 96.4, 44.9, 12.8. ESI-HRMS (positive mode, *m/z*) Calcd for C₁₄H₁₅NO₄: 261.1001 [CA – H]⁺; Found: 260.0995.

2.3. Synthesis and Characterization of DO3A-Gd

1,4,7-Tris(carboxymethyl)-1,4,7,10-tetraazacyclododecane (DO3A) and DO3A-Gd were synthesized according to the literature procedure [45,46]. ESI-HRMS (positive mode, *m/z*) of DO3A, Calcd for C₁₄H₂₇N₄O₆: 347.1931: [DO3A + H]⁺; Found: 347.1936; ESI-HRMS (positive mode, *m/z*) of DO3A-Gd, Calcd for C₁₄H₂₂GdN₄O₆: 500.0802 [DO3A-Gd][−]; Found: 500.0781.

2.4. Synthesis and Characterization of DO3A-Gd-CA

DO3A-Gd-CA was prepared by addition of 1.0 equiv. of [DO3A-Gd]Na to CA (10 μM) solution in CH₃CN-H₂O (9:1, *v/v*, pH = 7.4). ESI-HRMS (positive mode, *m/z*) of [DO3A-Gd-CA][−], Calcd for C₂₈H₃₇GdN₅O₁₀: 761.1803, Found: 761.1778.

2.5. General Procedures of Spectroscopic Detection

Stock solutions of CA (1 mM) were prepared in CH₃CN. Before spectroscopic measurements, the solution was freshly prepared by diluting the high concentration of stock solution to corresponding solution (10 μM, CH₃CN:H₂O = 9:1, pH = 7.4). DO3A-Gd-CA stock solution for anions sensing was prepared in situ by addition of 1.0 equiv. of [DO3A-Gd]Na to CA (10 μM) solution in CH₃CN-H₂O (9:1, *v/v*, pH = 7.4). Each time, a 3 mL solution of probe was filled in a quartz cell of 1 cm optical path length, and different stock solutions of cations were added into the quartz cell gradually by using a micro-syringe. Excitation wavelength for CA was 408 nm.

2.6. Association Constant Calculation

The Benesi-Hildebrand equation was used as shown below [47].

$$\frac{1}{F_0 - F} = \frac{1}{K_a(F_0 - F_{\min})[\text{DO3A-Gd}]} + \frac{1}{F_0 - F_{\min}}$$

where *F* and *F*₀ represent the fluorescence emission at 460 nm of CA in the presence and absence of [DO3A-Gd][−], respectively, *F*_{min} is the saturated fluorescence intensity.

2.7. MRI Experiment

Male 8-week-old mice were purchased from the Animal Experiment Center of Dalian Medical University. All live mice experiments were performed in compliance with the relevant laws and institutional guidelines.

All MR relaxivity measurements were performed on a MesoMR23-060H-I Analyzing & Imaging system (Shanghai Niumag Corp.). The specific relaxivity values of r_1 were calculated through the curve fitting of $1/T_1$ (s^{-1}) vs. the concentration of DO3A-Gd-CA (0.2 mM). T_1 -weighted MR images were acquired using a multi-slice gradient echo sequence.

3. Results

3.1. Synthesis and Photophysical Characterization of DO3A-Gd-CA in Solution

The formation of DO3A-Gd-CA was investigated by recording the changes in UV-Vis absorption and fluorescence spectra. As shown in Figure 1, consistent with the free coumarin derivative, CA displayed a major absorption maximum at 402 nm in aqueous medium ($CH_3CN:H_2O = 9:1$, $pH = 7.4$) [48]. In the presence of an increasing amount of $[DO3A-Gd]^-$ (0–15 μM), an obvious bathochromic-shift in the absorption band from 402 nm to 430 nm and an increase in the absorption at 430 nm were noted, which could be assigned to the complexation of CA with Gd(III) center.

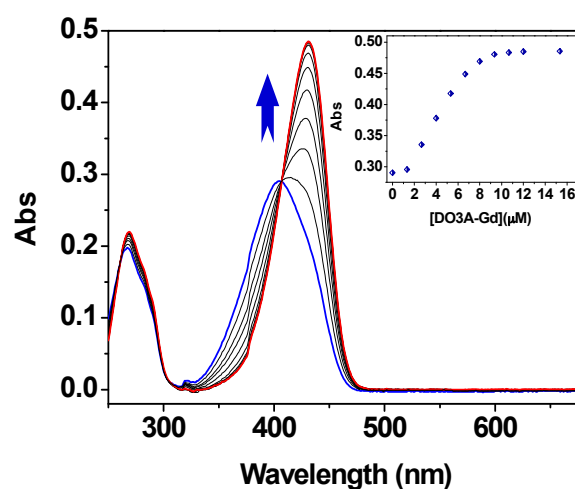


Figure 1. UV-Vis absorption spectra of CA (10 μM) in the presence of increasing amount of DO3A-Gd (0–15.0 μM) in CH_3CN-H_2O (9:1, v/v , $pH = 7.4$). Insert: The maximum absorbance band of CA at 430 nm against the concentrations of DO3A-Gd.

The complexation of CA with $[DO3A-Gd]^-$ was further studied by the analysis of fluorescence titration. CA displayed strong fluorescence at 460 nm in CH_3CN-H_2O (9:1, v/v , $pH = 7.4$). As expected, the fluorescence intensity of CA decreased gradually with a 12 nm bathochromic-shift in the emission band in the presence of an incremental addition of $[DO3A-Gd]^-$. The fluorescence intensity reached a constant value when 12 μM fluoride ion was added (Figure 2, insert). The decrease of fluorescence intensity (more than 81.5% fluorescence quenching) and bathochromic-shift of emission wavelength suggested the formation of the complex DO3A-Gd-CA [49,50]. Based on the 1:1 binding mode, the association constant (K_a) was evaluated to be $4.3 \times 10^3 M^{-1}$ using the Benesi–Hildebrand method (Figure S6) [51]. Furthermore, no obvious changes of the fluorescent intensities within 13 h, indicating that DO3A-Gd-CA is reliable under the test condition (Figure S7). The proposed structure of DO3A-Gd-CA was further confirmed by ESI-HRMS. As shown in Figure S8, analysis of the solution of DO3A-Gd-CA revealed the presence of a peak assigned to $[DO3A-Gd-CA]^-$ at $m/z = 761.1778$, indicating the formation of the expected 1:1 stoichiometry complex between DO3A-Gd and CA.

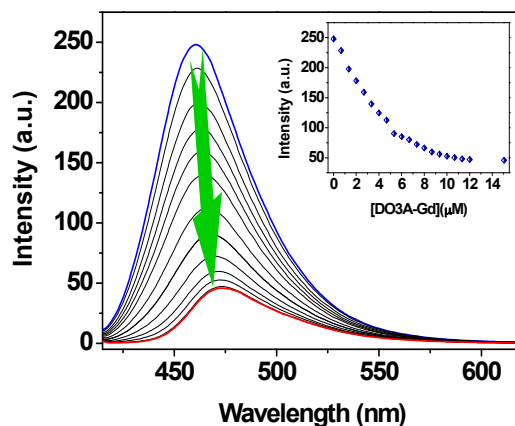


Figure 2. Fluorescence spectra of CA (10 μM) in $\text{CH}_3\text{CN-H}_2\text{O}$ (9:1, v/v , $\text{pH} = 7.4$) in the presence of different amounts of DO3A-Gd (0–15.0 μM). Insert: Fluorescence intensities of CA at 460 nm as a function of the concentration of DO3A-Gd. Excitation was performed at 408 nm.

3.2. Spectroscopic Studies of DO3A-Gd-CA towards Fluoride Ion in Aqueous Medium

By virtue of the high affinity of gadolinium(III) center and fluoride ions, fluoride is expected to replace the coordinated CA ligand [52], resulting the significant changes in UV-Vis and fluorescence spectra of CA, by which fluorescence detection of fluoride ion could be achieved. The stock solution of DO3A-Gd-CA for anion sensing was prepared in situ by the addition of 1.0 equiv. of $[\text{DO3A-Gd}]^-$ to CA solution (10 μM) in $\text{CH}_3\text{CN-H}_2\text{O}$ (9:1, v/v , $\text{pH} = 7.4$). The displacement approach was firstly investigated by UV-Vis spectra titration analysis. The major absorption band of DO3A-Gd-CA (10 μM) at 430 nm decreased and the absorption peak assigned to free CA at 402 nm emerged by the addition of 0–200 μM tetrabutylammonium fluoride ($n\text{-Bu}_4\text{NF}$) to the DO3A-Gd-CA solution (Figure 3). The final absorption spectrum was in agreement with the native CA in identical conditions (Figure S9a), which corroborated the results of the decomplexing of DO3A-Gd-CA in the presence of fluoride ion. The changes of absorption spectra of DO3A-Gd-CA in the presence of other physiologically and environmentally important anions, such as Br^- , I^- , AcO^- , HSO_4^- , NO_3^- , OH^- and H_2PO_4^- were then evaluated by UV-Vis analysis. As illustrated in Figure 4, obvious changes in UV-Vis spectra were obtained upon the addition of fluoride ions, instead of other anions even at high concentrations (concentration of Cl^- , PO_4^{3-} are 100 mM and 1 mM, respectively). This result indicates that DO3A-Gd-CA is specific toward fluoride ions over other competitive anions.

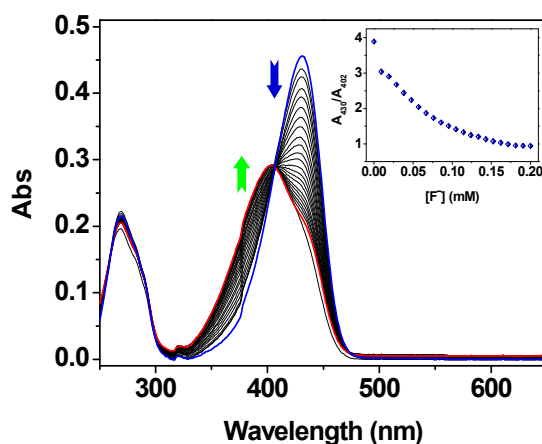


Figure 3. UV-Vis absorption spectra of DO3A-Gd-CA (10 μM) in the presence of increasing concentrations of fluoride ions (0–200 μM) in $\text{CH}_3\text{CN-H}_2\text{O}$ (9:1, v/v , $\text{pH} = 7.4$). Insert: Ratiometric changes of absorbance band of CA (A_{430}/A_{402}) as a function of fluoride ions concentrations.

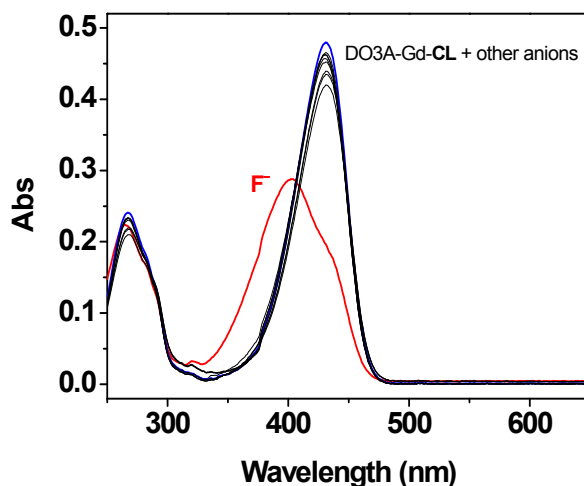


Figure 4. UV-Vis absorption spectra of DO3A-Gd-CA (10 μM) in the presence of various anions (200 μM) in $\text{CH}_3\text{CN-H}_2\text{O}$ (9:1, v/v , $\text{pH} = 7.4$): H_2PO_4^- (0.2 mM), PO_4^{3-} (1 mM), HSO_4^- (0.2 mM), Br^- (0.2 mM), I^- (0.2 mM), NO_3^- (0.2 mM), OH^- (0.2 mM), AcO^- (0.2 mM), Cl^- (100 mM), F^- (0.2 mM).

To evaluate the capability of DO3A-Gd-CA as the fluorescence probe for fluoride ions, emission spectra of DO3A-Gd-CA were then investigated. As shown in Figure 5, DO3A-Gd-CA presented a weak fluorescence emission. Upon the addition of fluoride ion, the maximum emission wavelength of DO3A-Gd-CA at 472 nm was gradually shifted to 460 nm, accompanied by an increase in fluorescence intensity. When 200 μM fluoride ion was added, the fluorescence intensity increased to a maximum value. The intensity and overall pattern of the emission spectrum closely match those of native CA state, indicating the liberation of coordinated CA ligand (Figure S9b). Job's plots of the fluorescence emission variation at 460 nm against the mole fraction of fluoride ions clearly showed the inflection point at 0.67 (Figure S10), which supported that DO3A-Gd-CA binding fluoride ion with 1:2 binding stoichiometry. The fluoride-induced replacement process was further verified by HRMS. Upon the addition of fluoride ions into the aqueous solution of DO3A-Gd-CA, the peak of $[\text{DO3A-Gd-CA}]^-$ at $m/z = 761.1778$ disappeared, and a new peak at $m/z = 260.0930$ assigned to $[\text{CA-H}^+]^-$ was emerged, indicating that the binding between fluoride ions with Gd(III) centers led to the release of CA (Figure S11). To evaluate the selectivity of DO3A-Gd-CA toward fluoride ion against other anions, the changes in fluorescence of DO3A-Gd-CA were examined in the presence of 0.2 mM various anions (Br^- , I^- , H_2PO_4^- , HSO_4^- , AcO^- , NO_3^- , OH^- , AcO^-) and 100 mM Cl^- , 1 mM PO_4^{3-} . The maximum emission of DO3A-Gd-CA significantly increased in the presence of fluoride ions exclusively, whereas other anions did not induce any detectable fluorescence enhancement (Figure 6). To further verify the excellent selectivity for fluoride ions, the competitive experiments were conducted by the addition of 0.2 mM fluoride ion to the mixture of DO3A-Gd-CA and diverse coexisting anions. As shown in Figure 6, negligible effects on the detection of fluoride ions were found in the presence of various competitive anions, indicating DO3A-Gd-CA is a fluorescence probe specific for fluoride ion detection [53]. The excellent selectivity to fluoride ions is partly due to the highest affinity to gadolinium(III) center compared to other anionic analytes [54]. The relative fluorescence intensity of DO3A-Gd-CA is linearly proportional to fluoride ions concentration of 0–30 μM (Figure S12), and the detection limit was calculated to be 8 μM based on a $3\sigma/\text{slope}$ under experimental conditions, which is low enough for fluoride ion sensing in aqueous medium and biological systems [55].

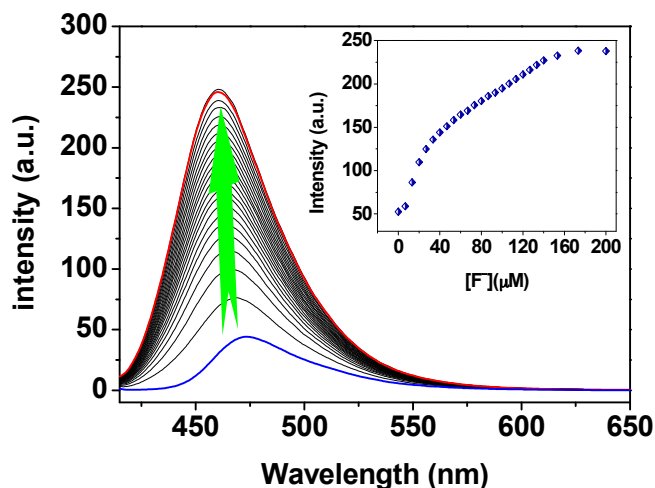


Figure 5. Fluorescence spectra of DO3A-Gd-CA (10 μM) in the presence of different concentrations of fluoride ion (0–200 μM). Insert: Fluorescence intensities of DO3A-Gd-CA (10 μM) at 460 nm as a function of fluoride ions concentration (0–200 μM). Excitation was performed at 408 nm.

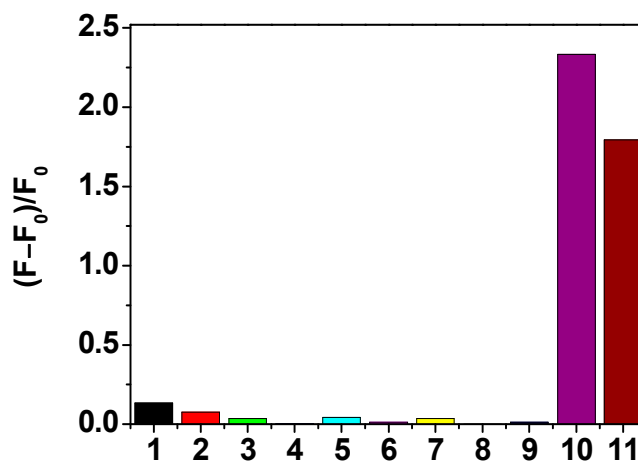


Figure 6. Changes in fluorescence intensity of DO3A-Gd-CA (10 μM) toward fluoride ion in the presence of various competing anions in $\text{CH}_3\text{CN-H}_2\text{O}$ (9:1, v/v , $\text{pH} = 7.4$): 1. H_2PO_4^- (0.2 mM), 2. PO_4^{3-} (1 mM), 3. HSO_4^- (0.2 mM), 4. Br^- (0.2 mM), 5. I^- (0.2 mM), 6. NO_3^- (0.2 mM), 7. OH^- (0.2 mM), 8. AcO^- (0.2 mM), 9. Cl^- (100 mM), 10. F^- (0.2 mM), and 11. All anions mixed. The intensities were recorded at 460 nm, excitation at 408 nm.

3.3. MRI Responses of DO3A-Gd-CA towards Anions in Aqueous Medium and In Vivo

The longitudinal relaxivity (r_1) of DO3A-Gd-CA towards fluoride ions was further investigated by a MesoMR23-060H-I Analyzing & Imaging system at 25 $^\circ\text{C}$. As shown in Figure 7, DO3A-Gd-CA (0.2 mM) exhibited relatively low longitudinal relaxivity ($r_1 = 1.67 \text{ mM}^{-1}\cdot\text{s}^{-1}$), suggesting that no inner-sphere water molecule was bonded to Gd(III) ion arising from the complexation of EDTA-Gd with CA ($q = 0$) [56]. Upon the addition of fluoride ion into the aqueous solution containing EDTA-Gd-CA (0.2 mM), the relaxivity increased to $2.957 \text{ mM}^{-1}\cdot\text{s}^{-1}$ (Figure 7), which closely matched the native EDTA-Gd state (Figure S13). The result demonstrated the replacement of coordination CA in the presence of fluoride ions. In addition, the corresponding T_1 -weighted images of DO3A-Gd-CA (0.2 mM) presented a continuous increase in spot brightness with increasing fluoride ion concentrations (Figure 7 insert). The increase in longitudinal relaxivity (r_1) demonstrated the applicability of DO3A-Gd-CA as an efficient T_1 MRI probe.

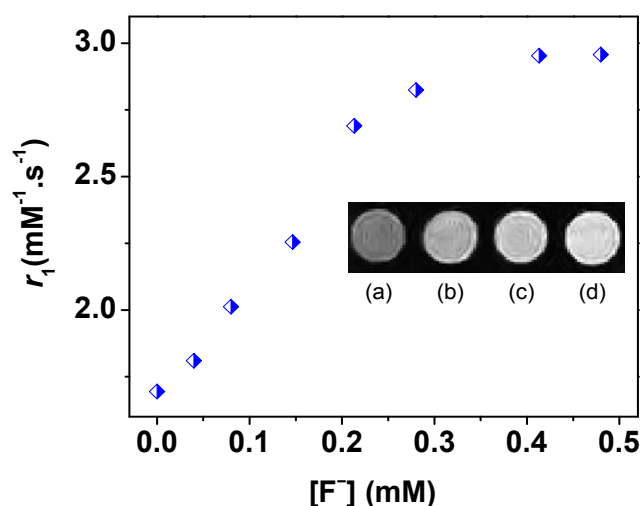


Figure 7. Changes in the longitudinal relaxivity (r_1) of DO3A-Gd-CA (0.2 mM) as a function of the fluoride ion concentration (0–0.5 mM) in CH₃CN-H₂O (9:1, v/v , pH = 7.4). Insert: T₁-weighted MR images of DO3A-Gd-CA recorded versus different concentrations of fluoride ion: (a) 0 mM; (b) 0.1 mM; (c) 0.3 mM; (d) 0.5 mM.

The changes in relaxivity of DO3A-Gd-CA were fluoride-specific over other physiologically important anions including Br⁻, I⁻, H₂PO₄⁻, HSO₄⁻, AcO⁻, NO₃⁻, OH⁻, AcO⁻, Cl⁻ (100 mM) and PO₄³⁻ (1 mM) (Figure 8). In addition, a distinctly increased imaging intensity in the presence of 0.5 mM fluoride ions was obtained, whereas no obvious differences were observed upon addition of other competitive anions (Figure 8, insert). In order to investigate the feasibility of DO3A-Gd-CA for the in vivo magnetic resonance imaging (MRI), the long-term cellular toxicity of DO3A-Gd-CA was evaluated by means of a MTT assay [57,58]. The MDA-MB-231 cell viabilities remained more than 80% at a high concentration of 200 μM even with an incubation time of 24 h, demonstrating the low cytotoxicity of DO3A-Gd-CA (Figure S14). In addition, the suitable pH range for DO3A-Gd-CA was evaluated to be 3.0–11.0, suggested that the probe is suitable for application under physiological conditions (Figure S15).

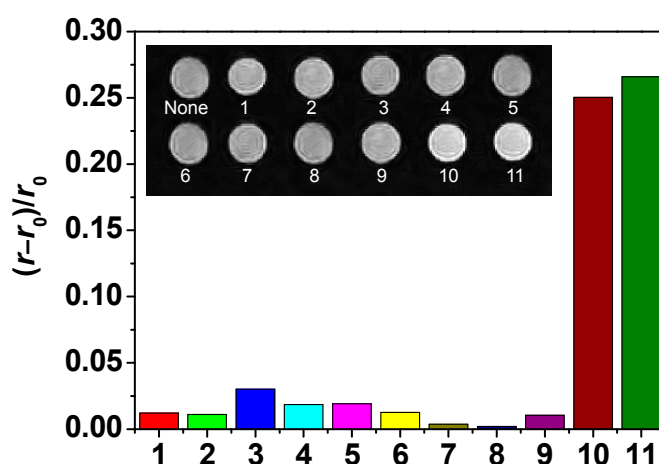


Figure 8. Longitudinal relaxivity (r_1) responses of DO3A-Gd-CA (0.2 mM) to various anions of interest (0.5 mM) in CH₃CN-H₂O (9:1, v/v , pH = 7.4). Insert: T₁-weighted MR images (T₁ measurements at a proton frequency of 20 MHz) of DO3A-Gd-CA (0.2 mM) in the presence of (1) Br⁻ (0.5 mM); (2) I⁻ (0.5 mM); (3) Cl⁻ (100 mM); (4) PO₄³⁻ (1.0 mM); (5) H₂PO₄⁻ (0.5 mM); (6) HSO₄⁻ (0.5 mM); (7) NO₃⁻ (0.5 mM); (8) OH⁻ (0.5 mM); (9) AcO⁻ (0.5 mM); (10) F⁻ (0.5 mM); and (11) All anions mixture.

Then, *in vivo* MRI experiments were studied using a 0.5 T MRI instrument. As shown in Figure 9b, after the injection of DO3A-Gd-CA (0.2 mM), a 40.1% contrast enhancement at the site of injection was observed compared with the baseline of the pre-injection image (Figure 9a). Further injection of fluoride ions (0.2 mL, 0.5 mM) into the hind legs of the mice led to the significant contrast effect of T_1 -weighted MR images in the areas of interest (Figure 9c). To demonstrate the potential applications of DO3A-Gd-CA in biomedical diagnosis fields, the proposed probe was subcutaneously injected into one hind leg of mouse and then imaged at different time points, respectively. As shown in Figure S16, the successive bright MRI action of the DO3A-Gd-CA on mice model was achieved at four representative time points, even after 12 h, suggesting that the contrast agents could continuously improve contrast in tissues and have a relatively longer blood circulation time. The results of images demonstrated that DO3A-Gd-CA could serve as a MRI probe for imaging of fluoride ions *in vivo*.

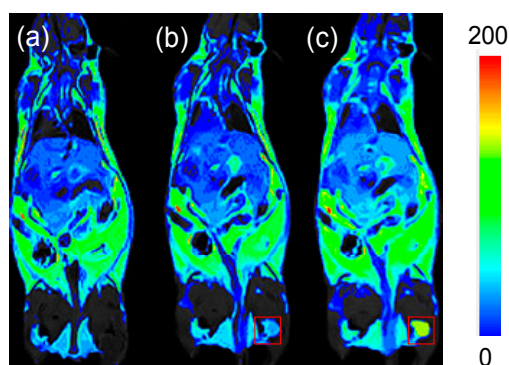


Figure 9. T_1 -weighted MR pseudocolor images of living white mice injection of: (a) Control group; (b) DO3A-Gd-CA (0.2 mL, 0.2 mM) only; (c) DO3A-Gd-CA (0.2 mL, 0.2 mM) + 0.5 mM fluoride ions.

4. Conclusions

In summary, we reported the design and synthesis of a novel mononuclear nine-coordinate complex, DO3A-Gd-CA as fluoride-specific fluorescence and MRI dual-modal probe. Upon the addition of fluoride ions to the aqueous solution of DO3A-Gd-CA, the replacement of the coordination aromatic carboxylic acid (CA) led an increase in longitudinal relaxivity (r_1) and an enhancement in fluorescence intensity, realizing switch-on dual-modal responses towards fluoride ions in water medium. The desirable features of DO3A-Gd-CA, such as high sensitivity, suitability at physiological pH, favorable dynamical stability and low cytotoxicity encouraged us to further evaluate its potential biological applications. *In vivo* magnetic resonance imaging (MRI) in mice indicates that DO3A-Gd-CA can be potentially used as a powerful tool for the detection of fluoride ions in live systems. Given these promising results, we believe that DO3A-Gd-CA is valuable both in methodology and potential application, which provides a new flexible strategy for the rational design of bimodal or multimodal probes for anion sensing.

Supplementary Materials: The following are available online at <http://www.mdpi.com/1424-8220/16/12/2165/s1>, Figures S1 and S2: NMR of CA, Figure S3–S5, S8, S11: HR MS characterizations, Figure S6: Benesi-Hildebrand plot, Figure S7: Stability of DO3A-Gd-CA, Figure S9: UV-Vis and emission spectra of CA sequential upon addition of $[DO3A-Gd]^-$ and fluoride ion, Figure S10: Job's plot, Figure S12: Linear relationship, Figure S13: Changes in the r_1 of DO3A-Gd as a function of the CA concentration, Figure S14: Cell viabilities, Figure S15: Influence of pH on DO3A-Gd-CA, Figure S16: Resident time of DO3A-Gd-CA in mice.

Acknowledgments: This work is supported by the National Natural Science Foundation of China (No. 21301011, 21601076), the Key Laboratory Program of Educational Department of Liaoning Province (LZ2015047), Natural Science Foundation of Liaoning Province (No. 201602400).

Author Contributions: Qingtao Meng conceived and designed the experiments, wrote the paper; Yue Wang and Huan Feng performed the synthesis and test experiments; Run Zhang contributed the cytotoxicity measurement; Renfeng Song and Ke Guo were involved in analyzing the data; Haijun Chi contributed to the high resolution MS spectra characterization; Zhiqiang Zhang contributed to manuscript revision.

Conflicts of Interest: The authors declare no conflict of interest.

References

1. Wang, H.; Wu, H.; Shen, H.; Geng, S.; Wang, B.; Wang, Y.; Ma, X.; Lid, G.; Tan, M. A bimodal MRI and NIR liposome nanoprobe for tumor targeted molecular imaging. *J. Mater. Chem. B* **2015**, *3*, 8832–8841. [[CrossRef](#)]
2. Zheng, X.; Tang, H.; Xie, C.; Zhang, J.; Wu, W.; Jiang, X. Tracking cancer metastasis in vivo by using an iridium-based hypoxia-activated optical oxygen nanosensor. *Angew. Chem. Int. Ed.* **2015**, *54*, 8094–8099. [[CrossRef](#)] [[PubMed](#)]
3. Zhou, Z.; Han, Z.; Lu, Z.-R. A targeted nanoglobular contrast agent from host-guest self-assembly for MR cancer molecular imaging. *Biomaterials* **2016**, *85*, 168–179. [[CrossRef](#)] [[PubMed](#)]
4. Munge, B.S.; Coffey, A.L.; Doucette, J.M.; Somba, B.K.; Malhotra, R.; Patel, V.; Gutkind, J.S.; Rusling, J.F. Nanostructured immunosensor for attomolar detection of cancer biomarker interleukin-8 using massively labeled superparamagnetic particles. *Angew. Chem. Int. Ed.* **2011**, *50*, 7915–7918. [[CrossRef](#)] [[PubMed](#)]
5. Pu, K.; Chattopadhyay, N.; Rao, J. Recent advances of semiconducting polymer nanoparticles in in vivo molecular imaging. *J. Control. Release* **2016**, *240*, 312–322. [[CrossRef](#)] [[PubMed](#)]
6. Xie, Z.; Li, S.; Yang, K.; Xu, B.; Ren, Q. Evaluation of a wobbling method applied to correcting defective pixels of CZT detectors in SPECT imaging. *Sensors* **2016**, *16*, 772. [[CrossRef](#)] [[PubMed](#)]
7. Lee, D.-E.; Koo, H.; Sun, I.-C.; Ryu, J.H.; Kim, K.; Kwon, I.C. Multifunctional nanoparticles for multimodal imaging and theragnosis. *Chem. Soc. Rev.* **2012**, *41*, 2656–2672. [[CrossRef](#)] [[PubMed](#)]
8. Weissleder, R.; Pittet, M.J. Imaging in the era of molecular oncology. *Nature* **2008**, *452*, 580–589. [[CrossRef](#)] [[PubMed](#)]
9. Pröhla, M.; Schuberta, U. S.; Weigand, W.; Gottschaldta, M. Metal complexes of curcumin and curcumin derivatives for molecular imaging and anticancer therapy. *Coord. Chem. Rev.* **2016**, *307*, 32–41. [[CrossRef](#)]
10. Zhang, X.; Bi, A.; Gao, Q.; Zhang, S.; Huang, K.; Liu, Z.; Gao, T.; Zeng, W. Advances of molecular imaging for monitoring the anatomical and functional architecture of the olfactory system. *ACS Chem. Neurosci.* **2016**, *7*, 4–14. [[CrossRef](#)] [[PubMed](#)]
11. Glunde, K.; Artemov, D.; Penet, M.-F.; Jacobs, M.A.; Bhujwala, Z.M. Magnetic resonance spectroscopy in metabolic and molecular imaging and diagnosis of cancer. *Chem. Rev.* **2010**, *110*, 3043–3059. [[CrossRef](#)] [[PubMed](#)]
12. Yang, T.; Liu, Q.; Pu, S.; Dong, Z.; Huang, C.; Li, F. Fluorophore-photochrome co-embedded polymer nanoparticles for photoswitchable fluorescence bioimaging. *Nano Res.* **2012**, *5*, 494–503. [[CrossRef](#)]
13. Jennings, L.E.; Long, N.J. ‘Two is better than one’—Probes for dual-modality molecular imaging. *Chem. Commun.* **2009**, 3511–3524. [[CrossRef](#)] [[PubMed](#)]
14. Guo, K.; Berezin, M.Y.; Zheng, J.; Akers, W.; Lin, F.; Teng, B.; Vasalatiy, O.; Gandjbakhche, A.; Griffiths, G.L.; Achilefu, S. Near infrared-fluorescent and magnetic resonance imaging molecular probe with high T₁ relaxivity for in vivo multimodal imaging. *Chem. Commun.* **2010**, *46*, 3705–3707. [[CrossRef](#)] [[PubMed](#)]
15. Quea, E.L.; Chang, C.J. Responsive magnetic resonance imaging contrast agents as chemical sensors for metals in biology and medicine. *Chem. Soc. Rev.* **2010**, *39*, 51–60. [[CrossRef](#)] [[PubMed](#)]
16. Berdichevski, A.; Yameen, H.S.; Dafni, H.; Neeman, M.; Seliktar, D. Precise and in situ genetic humanization of 6 Mb of mouse immunoglobulin genes. *Proc. Natl. Acad. Sci. USA* **2015**, *112*, 5147–5152. [[CrossRef](#)] [[PubMed](#)]
17. Meng, Q.T.; Jia, H.M.; Succar, P.; Zhao, L.; Zhang, R.; Duan, C.Y.; Zhang, Z.Q. A highly selective and sensitive ON–OFF–ON fluorescen cechemosensor for cysteine detection in endoplasmic reticulum. *Biosens. Bioelectron.* **2015**, *74*, 461–468. [[CrossRef](#)] [[PubMed](#)]
18. Lei, Z.; Yang, Y. A concise colorimetric and fluorimetric probe for sarin related threats designed via the “Covalent-Assembly” approach. *J. Am. Chem. Soc.* **2014**, *136*, 6594–6597. [[CrossRef](#)] [[PubMed](#)]
19. Lee, K.; Dzubeck, V.; Latshaw, L.; Schneider, J.P. De novo designed peptidic redox potential probe: Linking sensitized emission to disulfide bond formation. *J. Am. Chem. Soc.* **2004**, *126*, 13616–13617. [[CrossRef](#)] [[PubMed](#)]
20. Babailov, S.P. Thulium diketonate as NMR paramagnetic probe for moderately fast molecular dynamics and supersensitive reagent for in situ control of temperature. *Sens. Actuators B* **2016**, *233*, 476–478. [[CrossRef](#)]

21. Louie, A. Multimodality Imaging Probes: Design and Challenges. *Chem. Rev.* **2010**, *110*, 3146–3195. [[CrossRef](#)] [[PubMed](#)]
22. Kobayashi, H.; Longmire, M.R.; Ogawa, M.; Choyke, P.L. Rational chemical design of the next generation of molecular imaging probes based on physics and biology: Mixing modalities, colors and signals. *Chem. Soc. Rev.* **2011**, *40*, 4626–4648. [[CrossRef](#)] [[PubMed](#)]
23. Wang, Y.; Song, R.F.; Guo, K.; Meng, Q.T.; Zhang, R.; Kong, X.; Zhang, Z.Q. A gadolinium(III) complex based dual-modal probe for MRI and fluorescence sensing of fluoride ions in aqueous medium and in vivo. *Dalton Trans.* **2016**, *45*, 17616–17623. [[CrossRef](#)] [[PubMed](#)]
24. Ngo, H.T.; Liu, X.; Jolliffe, K.A. Anion recognition and sensing with Zn(II)–dipicolylamine complexes. *Chem. Soc. Rev.* **2012**, *41*, 4928–4965. [[CrossRef](#)] [[PubMed](#)]
25. Gupta, A.S.; Paul, K.; Luxami, V. Ratiometric fluorescent chemosensor for fluoride ion based on inhibition of excited state intramolecular proton transfer. *Spectrochim. Acta A* **2015**, *138*, 67–72. [[CrossRef](#)] [[PubMed](#)]
26. Pillai, A.B.; Varghese, B.; Madhusoodanan, K.N. Design and Development of Novel Sensors for the Determination of Fluoride in Water. *Environ. Sci. Technol.* **2012**, *46*, 404–409. [[CrossRef](#)] [[PubMed](#)]
27. Ren, X.X.; Wang, Y.; Meng, Q.T.; Jia, H.M.; Wang, Y.F.; Kong, X.F.; Duan, C.Y.; Zhang, Z.Q. A Coumarin-based Colorimetric and Fluorescent Chemosensor for the “Naked-eye” Detection of Fluoride ion in 100% Natural Water Medium Using Coated Chromatography Plates. *ChemistrySelect* **2016**, *1*, 4397–4402. [[CrossRef](#)]
28. Liu, X.; Xu, J.; Lv, Y.; Wu, W.; Liu, W.; Tang, Y. An ATP-selective, lanthanide complex luminescent probe. *Dalton Trans.* **2013**, *42*, 9840–9846. [[CrossRef](#)] [[PubMed](#)]
29. Mizukami, S.; Tonai, K.; Kaneko, M.; Kikuchi, K. Lanthanide-Based Protease Activity Sensors for Time-Resolved Fluorescence Measurements. *J. Am. Chem. Soc.* **2008**, *130*, 14376–14377. [[CrossRef](#)] [[PubMed](#)]
30. Efimov, N.N.; Koroteev, P.S.; Gavrikov, A.V.; Ilyukhin, A.B.; Dobrokhotova, Z.V.; Novotortsev, V.M. Magnetic Behavior of Carboxylate and β -Diketonate Lanthanide Complexes Containing Stable Organometallic Moieties in the Core-Forming Ligand. *Magnetochemistry* **2016**, *2*, 38. [[CrossRef](#)]
31. Vaněk, J.; Lubal, P.; Ševčíková, R.; Polášek, M.; Hermann, P. Mono(pyridine-N-oxide) analog of DOTA as a suitable organic reagent for a sensitive and selective fluorimetric determination of Ln(III) ions. *J. Lumin.* **2012**, *132*, 2030–2035. [[CrossRef](#)]
32. Tripier, R.; Platas-Iglesias, C.; Boos, A.; Morfin, J.-F.; Charbonnière, L. Towards Fluoride Sensing with Positively Charged Lanthanide Complexes. *Eur. J. Inorg. Chem.* **2010**, 2735–2745. [[CrossRef](#)]
33. Li, W.; Fraser, E.; Meade, T.J. A Calcium-Sensitive Magnetic Resonance Imaging Contrast Agent. *J. Am. Chem. Soc.* **1999**, *121*, 1413–1414. [[CrossRef](#)]
34. Major, J.L.; Boiteau, R.M.; Meade, T.J. Mechanisms of Zn^{II}-Activated Magnetic Resonance Imaging Agents. *Inorg. Chem.* **2008**, *47*, 10788–10795. [[CrossRef](#)] [[PubMed](#)]
35. Louie, Y.; Huber, M.M.; Ahrens, E.T.; Rothbacher, U.; Moats, R.; Jacobs, R.E.; Fraser, S.E.; Meade, T.J. In vivo visualization of gene expression using magnetic resonance imaging. *Nat. Biotechnol.* **2000**, *18*, 321–325. [[PubMed](#)]
36. Gunnlaugsson, T.; Harte, A.J.; Leonard, J.P.; Nieuwenhuyzen, M. Delayed lanthanide luminescence sensing of aromatic carboxylates using heptadentate triamide Tb(III) cyclen complexes: The recognition of salicylic acid in water. *Chem. Commun.* **2002**, *18*, 2134–2135. [[CrossRef](#)]
37. Wang, Y.; Jin, C.-W.; He, S.-M.; Ren, N.; Zhang, J.-J. Five novel lanthanide complexes with 2-chloroquinoline-4-carboxylic acid and 1,10-phenanthroline: Crystal structures, molecular spectra, thermal properties. *J. Mol. Struct.* **2016**, *1125*, 383–390. [[CrossRef](#)]
38. Girginova, P.I.; Pereira, L.C.J.; Coutinho, J.T.; Santos, I.C.; Almeida, M. Slow magnetic relaxation in lanthanide ladder type coordination polymers. *Dalton Trans.* **2014**, *43*, 1897–1903. [[CrossRef](#)] [[PubMed](#)]
39. Wang, Q.; Fan, Y.; Song, T.; Xu, J.; Wang, J.; Chai, J.; Liu, Y.; Wang, L.; Zhang, L. In situ synthesis of a series of lanthanide coordination polymers based on N-heterocyclic carboxylate ligands: Crystal structure and luminescence. *Inorg. Chim. Acta* **2015**, *438*, 128–134. [[CrossRef](#)]
40. Gai, Y.-L.; Xiong, K.-C.; Chen, L.; Bu, Y.; Li, X.-J.; Jiang, F.-L.; Hong, M.-C. Visible and NIR Photoluminescence Properties of a Series of Novel Lanthanide–Organic Coordination Polymers Based on Hydroxyquinoline–Carboxylate Ligands. *Inorg. Chem.* **2012**, *51*, 13128–13137. [[CrossRef](#)] [[PubMed](#)]
41. Choi, C.-L.; Yen, Y.-F.; Sung, H.H.-Y.; Siu, A.W.-H.; Jayarathne, S.T.; Wong, K.S.; Williams, I.D. Quantifying enhanced photoluminescence in mixed-lanthanide carboxylate polymers: Sensitization versus reduction of self-quenching. *J. Mater. Chem.* **2011**, *21*, 8547–8549. [[CrossRef](#)]

42. Plush, S.E.; Gunnlaugsson, T. Luminescent Sensing of Dicarboxylates in Water by a Bismacrocylic Dinuclear Eu(III) Conjugate. *Org. Lett.* **2007**, *9*, 1919–1922. [[CrossRef](#)] [[PubMed](#)]
43. Lo, L.-C.; Liao, Y.-C.; Kuo, C.-H.; Chen, C.-T. A Novel Coumarin-Type Derivatizing Reagent of Alcohols: Application in the CD Exciton Chirality Method for Microscale Structural Determination. *Org. Lett.* **2000**, *2*, 683–685. [[CrossRef](#)] [[PubMed](#)]
44. Nithyakumar, A.; Alexander, V. Synthesis, relaxivity, and in vitro fluorescence imaging studies of a novel d–f heterometallic trinuclear complex as a potential bimodal imaging probe for MRI and optical imaging. *Dalton Trans.* **2015**, *44*, 17800–17809. [[CrossRef](#)] [[PubMed](#)]
45. Faulkner, S.; Carrié, M.-C.; Pope, S.J.A.; Squire, J.; Beeby, A.; Sammes, P.G. Pyrene-sensitised near-IR luminescence from ytterbium and neodymium complexes. *Dalton Trans.* **2004**, *15*, 1405–1409. [[CrossRef](#)] [[PubMed](#)]
46. Meng, Q.T.; Shi, Y.; Wang, C.P.; Jia, H.M.; Gao, X.; Zhang, R.; Wang, Y.F.; Zhang, Z.Q. NBD-based fluorescent chemosensor for theselective quantification of copper and sulfide inan aqueous solution and living cells. *Org. Biomol. Chem.* **2015**, *13*, 2918–2926. [[CrossRef](#)] [[PubMed](#)]
47. Ishikawa, N.; Sugita, M.; Wernsdorfer, W. Quantum Tunneling of Magnetization in Lanthanide Single-Molecule Magnets: Bis(phthalocyaninato)terbium and Bis(phthalocyaninato)dysprosium Anions. *Angew. Chem. Int. Ed.* **2005**, *44*, 2931–2935. [[CrossRef](#)] [[PubMed](#)]
48. Wei, C.; Wang, R.; Wei, L.; Cheng, L.; Li, Z.; Xi, Z.; Yi, L. o-Fluorination of Aromatic Azides Yields Improved Azido-Based Fluorescent Probes for Hydrogen Sulfide: Synthesis, Spectra, and Bioimaging. *Chem. Asian J.* **2014**, *9*, 3586–3592. [[CrossRef](#)] [[PubMed](#)]
49. Choi, M.G.; Cha, S.; Lee, H.; Jeon, H.L.; Chang, S.-K. Sulfide-selective chemosignaling by a Cu²⁺ complex of dipicolylamine appended fluorescein. *Chem. Comm.* **2009**, *47*, 7390–7392. [[CrossRef](#)] [[PubMed](#)]
50. Peng, B.; Chen, W.; Liu, C.; Rosser, E.W.; Pacheco, A.; Zhao, Y.; Aguilar, H.C.; Xian, M. Fluorescent Probes Based on Nucleophilic Substitution-Cyclization for Hydrogen Sulfide Detection and Bioimaging. *Chem. Eur. J.* **2014**, *20*, 1010–1016. [[CrossRef](#)] [[PubMed](#)]
51. Meng, Q.T.; Jia, H.M.; Gao, X.; Wang, Y.; Zhang, R.; Wang, R.J.; Zhang, Z.Q. Reversible and Selective Fluorescence Detection of HistidineUsing a Naphthalimide-Based Chemosensing Ensemble. *Chem. Asian J.* **2015**, *10*, 2411–2418. [[CrossRef](#)] [[PubMed](#)]
52. Blackburn, O.A.; Routledge, J.D.; Jennings, L.B.; Rees, N.H.; Kenwright, A.M.; Beer, P.D.; Faulkner, S. Substituent effects on fluoride binding by lanthanide complexes of DOTA-tetraamides. *Dalton Trans.* **2016**, *45*, 3070–3077. [[CrossRef](#)] [[PubMed](#)]
53. Wang, F.; Wu, J.; Zhuang, X.; Zhang, W.; Liu, W.; Wang, P.; Wu, S. A highly selective fluorescent sensor for fluoride in aqueous solution based on the inhibition of excited-state intramolecular proton transfer. *Sens. Actuators B* **2010**, *146*, 260–265. [[CrossRef](#)]
54. Mizukami, S.; Nagano, T.; Urano, Y.; Odani, A.; Kikuchi, K. A fluorescent anion sensor that works in neutral aqueous solution for bioanalytical application. *J. Am. Chem. Soc.* **2002**, *124*, 3920–3925. [[CrossRef](#)] [[PubMed](#)]
55. Koteeswari, R.; Ashokkumar, P.; Malar, E.J.P.; Ramakrishnan, V.T.; Ramamurthy, P. Highly selective, sensitive and quantitative detection of Hg²⁺ in aqueous medium under broad pH range. *Chem. Commun.* **2011**, *47*, 7695–7697. [[CrossRef](#)] [[PubMed](#)]
56. Shen, C.; New, E.J. Promising strategies for Gd-based responsive magnetic resonance imaging contrast agents. *Curr. Opin. Chem. Biol.* **2013**, *17*, 158–166. [[CrossRef](#)] [[PubMed](#)]
57. Xie, N.; Feng, K.; Chen, B.; Zhao, M.; Peng, S.; Zhang, L.-P.; Tung, C.-H.; Wu, L.-Z. Water-soluble copolymeric materials: Switchable NIR two-photon fluorescence imaging agents for living cancer cells. *J. Mater. Chem. B* **2014**, *2*, 502–510. [[CrossRef](#)]
58. Shibu, E.S.; Sugino, S.; Ono, K.; Saito, H.; Nishioka, A.; Yamamura, S.; Sawada, M.; Nosaka, Y.; Biju, V. Singlet-oxygen-sensitizing near-infrared-fluorescent multimodal nanoparticles. *Angew. Chem. Int. Ed.* **2013**, *52*, 10559–10563. [[CrossRef](#)] [[PubMed](#)]

